J | P | S | T

http://jpst.irost.ir

Journal of Particle Science and Technology

IROST

Photocatalytic degradation of methyl orange using TiO_2:Mg^{2+}/zeolite composite under visible light irradiation

Afsaneh Mozayyeni, Jafar Mahmoudi*

School of Chemistry, Damghan University, Damghan, Iran

HIGHLIGHTS

- The TiO_2:Mg^{2+}/zeolite composite can degrade MO under visible light successfully.
- XRF, XRD, FTIR and SEM measurements were performed for structural properties.
- Addition of Mg in TiO_2/zeolite combination has significant effect on degradation.
- The photocatalyst is found to be reusable.

GRAPHICAL ABSTRACT

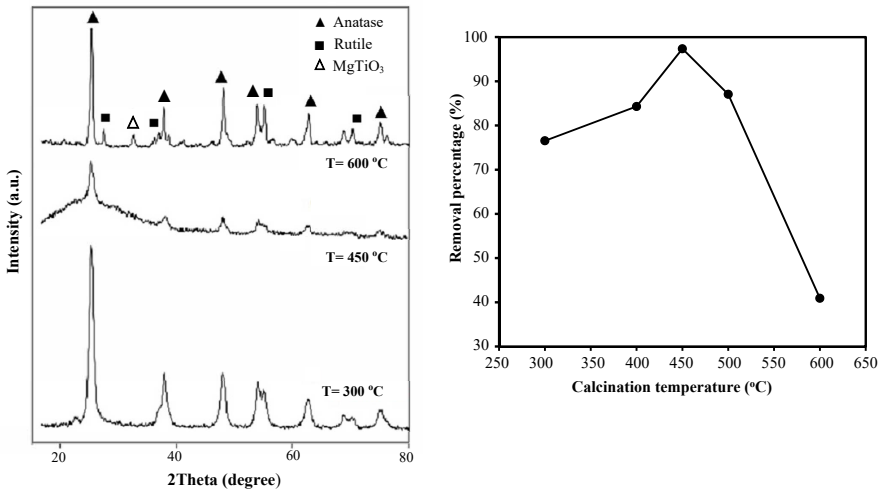

ARTICLE INFO

Article history:

Received 29 November 2019
Revised 16 May 2020
Accepted 22 June 2020

Keywords:

TiO_2
Mg
Zeolite
Methyl orange
Photocatalyst

ABSTRACT

Photodegradation of methyl orange was investigated using synthesized TiO_2:Mg^{2+}/zeolite as the photocatalyst. The photocatalyst was characterized by X-ray, XRF, FT-IR, and SEM. The photocatalytic activities of TiO_2:Mg^{2+}/zeolite samples were evaluated in the degradation of methyl orange under visible light irradiation. The appropriate content of Mg in the composite was obtained as 4.711 wt% with 100% removal of methyl orange in 50 minutes. The influence of irradiation time, catalyst concentration, pH, and calcination temperature on the photodegradation of methyl orange was investigated, and the appropriate amounts obtained for these parameters were 60 min, 5 g/l, 10, and 450 °C, respectively. The degradation of methyl orange over TiO_2:Mg^{2+}/zeolite was about 82% after five cycles, confirming the suitable reusability of the photocatalyst.

* *Corresponding author: Tel.: +9823-35220095 ; Fax: +9823-35220095 ; E-mail address: mahmoudi@du.ac.ir*
DOI: 10.22104/JPST.2020.3936.1162

1. Introduction

The use of synthetic dyes with complex structures and high chemical stability have recently increased, which could cause environmental pollution and health problems if the wastewater of these industries is left untreated [1-3]. Among the synthetic dyes existing in textile wastewater, azo dyes are very stable and barely degradable [4]. Azo dyes are organic compounds containing the functional group R−N=N−R′, in which the R and R′ are usually aryls. This functional wastewater group can be broken down into an aromatic amine, arylamine [5-7], which is poisonous, mutagenic, and carcinogenic, and therefore necessary to remove from wastewater [8].

There are various processes to remove dyeing pollutants from wastewater, such as chemical coagulation, adsorption, saturation, the membrane process, and ion exchang, and most of these processes are costly and have low efficiency [9-10]. The use of advanced oxidation methods in wastewater treatment has increased recently. The most conventional advanced oxidation methods include photocatalyst [11], electrochemical [12], electrocoagulation [13] and ultrasound [14] processes. For the non-selective and fast removal of pollutants in these processes, pollutants (specifically the organic ones) were decomposed by producing species with very high reactivity. In the mentioned methods, photocatalysis appears as an interesting approach for wastewater treatment using light radiation as a source of energy. Moreover, this method minimizes the production of hazardous byproducts [15-17]. Titanium dioxide is one of the most widely used photocatalysts due to its strong oxidizing power, chemical and physical stability, low cost, and non-toxicity. Rutile, anatase, and brookite are the three major phases of crystalline titanium dioxide, andrutile and anatase are tetragonal while brookite is orthorhombic [18-19]. In photocatalytic degradation of pollutants via TiO_2, a large number of electron-hole pairs are re-combined, and only a few migrate to the photocatalyst surface and participate in reduction-oxidation processes, which could reduce the efficiency of the process. Modification of TiO_2 with selected metal ions can improve the inter-surface charge transfer, delay the electron return, and stop electron-hole recombination. In addition to metal ions, different compounds such as zeolites, active carbon, perlite, alginat, etc. have been tested as the base for performing photocatalytic reactions [20]. Natural zeolites are popular as they are very inexpensive, accessible, and advantages such as their photochemical stability, porous structure, channels with the same size and order, high thermal stability, and absorption capacity as well as being environmentally-friendly [19,21]. In the present research, a low amount of zeolite is composite with titanium dioxide in order to reduce electron-hole recombination and increase the photocatalytic removal efficiency. Also, many authors [9-10] reduce electron-hole recombination by using prepared TiO_2 loaded metals oxide such as using MgO catalysts to study the photocatalytic reduction of nitrate in an aqueous solution.

In the present work, the TiO_2:Mg^{2+}/Zeolite composite is prepared as a suitable photocatalyst for the degradation of methyl orange dye. The photocatalysts were characterized by XRD, XRF, FESM, and FT-IR techniques. The influence of irradiation time, catalyst concentration, pH, Mg content, and calcination temperature on the photodegradation of methyl orange was also examined. The photocatalytic degradation of methyl orange was measured using a UV/Vis absorption spectrophotometer.

2. Experimental procedure

2.1. Materials

Clinoptilolite, a natural zeolite from Semnan, Iran, was prepared. Titanium isopropoxide (Sigma-Aldrich, 97%), ethanol (Merck, 99.9%), acetic acid (Merck, 99.5%), methyl orange (Sigma-Aldrich, >99%), magnesium nitrate (Merck, 99%), and deionized water were used throughout this study.

2.2. Preparation of TiO_2 sol

To prepare the TiO_2, 5 ml of titanium isopropoxide was added to 20 ml of ethanol, and then the solution was stirred for 30 min on a magnetic stirrer as described in [19]. Next, a solution containing 4.3 ml of acetic acid, 5 ml of ethanol, and 0.26 ml of water was poured into the precursor solution dropwise under strong stirring. After one hour, a clear yellow $TiO_2.xH_2O$ sol was formed.

2.3. Preparation of TiO_2:Mg^{2+}/zeolites

The detailed preparation process of TiO_2/zeolite is

described in [15-16]. The TiO_2:Mg^{2+}/zeolite composite was prepared as follows: First, 0.1 g of zeolite powder was mixed with the above $TiO_2.xH_2O$ sol under constant stirring. After 3h, different amounts of magnesium nitrate (2.827, 4.711, 9.422, and 14.342 wt% of Mg) were added into the above solution and stirred for 6 h on a magnetic stirrer. In the next step, a solution of an equal wt% of water and ethanol was poured into the above solution dropwise under strong stirring for 5 min to obtain a precipitate which was then dried in the oven at 120°C for 11 h. Finally, the dried powder was calcined at different temperatures (300, 450, and 600 °C) for 4 h.

2.4. Characterization of the photocatalyst

The chemical composition of the synthesized samples was identified by X-ray fluorescence analysis (XRF) on an S4 Explorer Bruker X-ray fluorescence spectrometer. An X-ray diffractometer (D8-Advance, Bruker AXS, Cu K_α, λ = 0.154 nm) was utilized to determine the crystalline structure of the synthesized samples. The infrared spectra of the photocatalysts were recorded using a Perkin Elmer Spectrum RXI FT-IR in the range of 400 to 4000 cm^{-1}. The samples were mixed with KBr powder and compressed into a pellet for analysis. Scanning electron microscopy (SEM) (JEOL, JSM 6490 LV) with an electron acceleration voltage of 20 kV was employed to determine the morphology of the synthesized samples.

2.5. Photocatalytic activity tests

Photocatalytic experiments were performed in a batch reactor equipped with a high-pressure Hg lamp (250 W) and a magnetic stirrer placed in the wooden chamber. Based on preliminary experiments for the degradation of methyl orange, in each experiment, 0.1 g of the photocatalyst was added into 20 ml of 10 ppm methyl orange aqueous solution. In the next step, the sample was exposed to visible light for 50 min under constant stirring. After the reaction ended, the suspension was centrifuged and filtered through a membrane filter to remove the photocatalyst particles. The remaining concentration of methyl orange was also analyzed by measuring the maximum absorbance at 465 nm using a UV–vis spectrophotometer (UV-1800, Shimadzu, Japan). All results are expressed as averaged values of duplicate tests. The methyl orange degradation percentage (X) was calculated using the Eq. (1).

$$X\,(\%) = [(C_0 - C_e)/C_0] \times 100 \quad (1)$$

where C_0 and C_e represent the initial concentration of the methyl orange solution and the concentration of methyl orange analyzed at the end of the reaction, respectively. To investigate the effected parameters on photodegradation of methyl orange, some experiments were carried out in triplicate to exclude exceptions in the measurements that could lead to wrong conclusions. The average deviation of the removal percentage of methyl orange for all performed experiments was about 1.15%.

3. Results and Discussion

3.1. XRF and XRD analyses

The chemical compositions and XRD pattern of clinoptilolite zeolite from the Semnan area in the range of 2θ = 5˚ to 80˚ are depicted in Fig. 1. The photocatalytic activity of zeolite depends on its structural properties and chemical composition. The main components of natural zeolites are Si and Al oxides. The molar ratio of Si to Al in zeolite is based on the XRF data of 5.6, indicating that it is classified as zeolite A [3]. Clinoptilolite zeolite has several characteristic peaks at 2θ = 9.63˚, 22.40˚, 26.71˚, 30.19˚, and 32.74˚ assigned to biotite ($K(Mg, Fe)_3AlSi_3O_{10}(F, OH)_2$), clinoptilolite ($(Na, K, Ca)_{2\text{-}3}Al_3(Al, Si)_2Si1_3O_{36}$, $12(H_2O)$), quartz (SiO_2), feldspar ($KAlSi_3O_8$-$NaAlSi_3O_8$-$CaAl_2Si_2O_8$), and dolomite ($CaMg(CO_3)_2$), respectively, which can be indexed for clinoptilolite XRD file with JCPDS No. 38-0237 and 38-1389 [4-6].

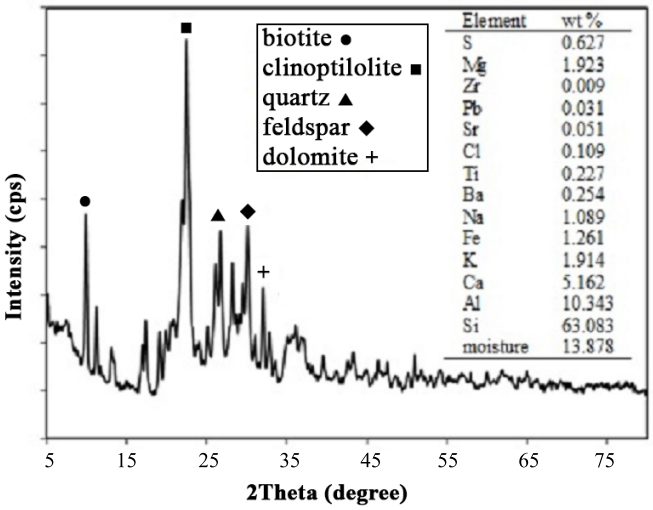

Fig. 1. The XRF result and the XRD pattern of clinoptilolite zeolite from the Semnan region of Iran.

Fig. 2 illustrates the chemical composition results and X-ray diffraction patterns for the synthesized TiO_2. In Fig. 2, strong diffraction peaks around 25˚, 38˚, 48˚, 62.5˚, and 75.1˚ are attributed to the TiO_2 in the anatase phase, which matches well with the PDF table (01-084-1285), (JCPDS No. 21-1272). Also, the XRD patterns exhibited weak diffraction peaks at 37˚ and 55˚, indicating a TiO_2 in the rutile phase, which matches well with the PDF table (01-088-1175), (JCPDS No. 65-0190). Based on this figure, the synthesized TiO_2 was mainly composed of the anatase phase. It was previously reported that, from among the crystalline forms of TiO2, anatase is the most photocatalytic phase in comparison with other phases [7].

Based on our preliminary experiments, combining zeolite with TiO_2 induced the enhancement of photocatalytic activity, and an appropriate zeolite content in the TiO_2/zeolite composite was obtained at about 10% by weight. In this study, we investigated the influence of effective parameters on the synthesis of the TiO_2:Mg^{2+}/zeolite composite in order to improve photocatalytic efficiency. The X-ray diffraction patterns of the TiO_2:Mg^{2+}/zeolite composite synthesized with different amounts of magnesium nitrate are illustrated in Fig. 3. As can be seen, diffraction peaks appearing around 2θ = 25.4˚, 38.1˚, 48.1˚, 62.5˚, and 75.1˚ can be assigned to the anatase phase, and diffraction peaks at 2θ = 56.6˚ and 69.9˚ correspond to the characteristic peaks of rutile. According to the diffraction patterns, by increasing the amount of magnesium nitrate to an appropriate amount (4.711 wt% of Mg), the intensities of the rutile phase diffraction peaks decreased. Also, the addition of Mg and zeolite slightly shifted the peak positions towards a higher diffraction angle. Based on patterns, anatase was determined to be the dominant phase, which is useful due to its suitable performance in the separation of electron-hole pairs and the higher photocatalytic activity. Based on Fig. 3, after adding the appropriate amount of Mg, the amount of the rutile phase increased. As reported in [23], the XRD pattern of the MgO has two main diffraction peaks around 43.5˚ and 63˚ (JCPDF card No. 79-0612). While, Ferri *et al.* [9] reported that three broad diffraction peaks of $MgTiO_3$ at a calcination temperature of 450 °C appeared in 2θ = 33˚, 43˚, and 62.5˚. Based on Fig. 3, it seems that due to the overlap of the diffraction peaks of MgO and TiO_2 peaks around 2˚ = 63˚, no particular phases of MgO in the XRD spectra of TiO_2:Mg^{2+}/zeolite samples (especially TiO_2:Mg^{2+}/zeolite with 14.342 wt% of Mg) were observed at 450 °C of calcination temperature. For $MgTiO_3$, no peaks were observed at 2θ = 33˚ or 43˚, but it seems that the overlapping accrued at around 2θ = 63˚.

Fig. 4 depicts the XRD patterns of the TiO_2:Mg^{2+}/zeolite photocatalyst at various calcination temperatures.

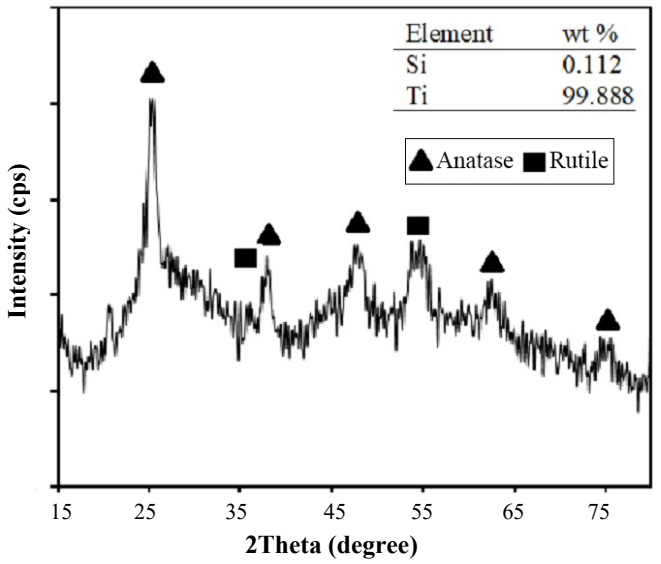

Fig. 2. (a) Architecture and (b) computational flowchart of ANN-MPSO implementation structure and inthe predicton of CNTs length as a function of FC-CVD practical parameters.

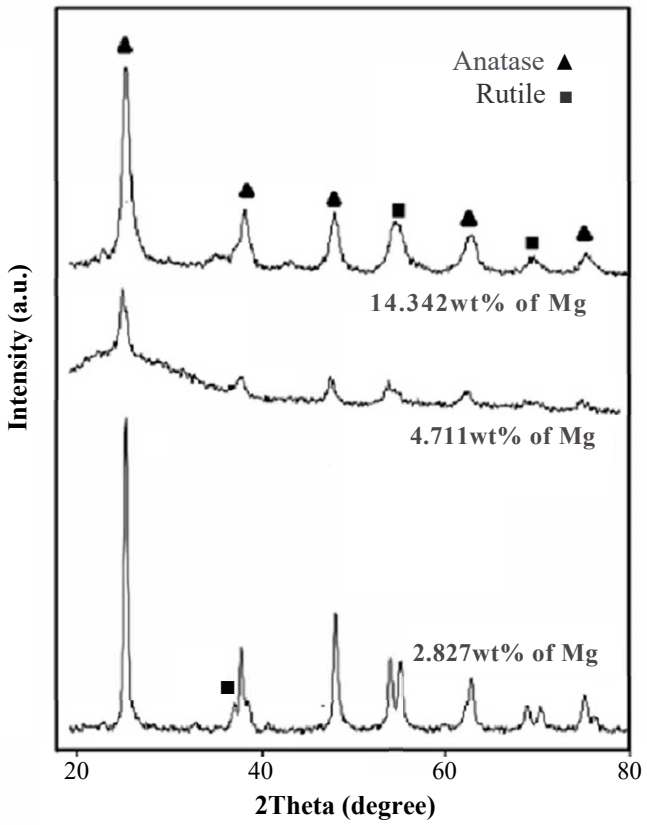

Fig. 3. The XRD spectra of TiO_2:Mg^{2+}/zeolite composites synthesized with different amounts of Mg.

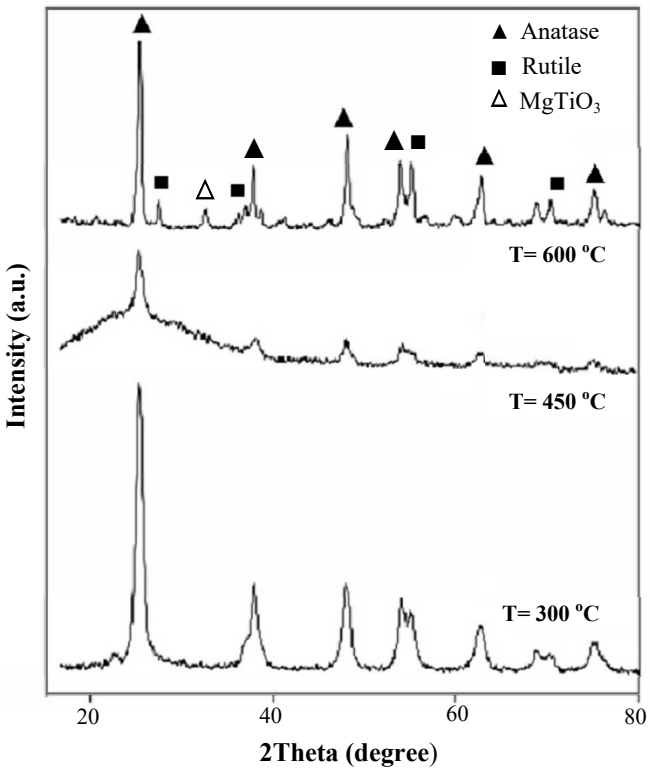

Fig. 4. The XRD spectrum of the TiO_2:Mg^{2+}/zeolite composites synthesized at various calcination temperatures.

According to the diffraction patterns, anatase and rutile peaks were observed in the synthesized sample calcined at 300 °C. However, when the temperature was increased to 450 °C the intensities of some diffraction peaks of the rutile phase (2θ = 37˚ and 56˚) decreased or disappeared. J. Krysa *et al.* [7] reported that at a calcination temperature lower than 600 °C, the anatase phase is the main phase of the synthesized TiO_2, and in some cases, pure anatase is formed. Moreover, the intensities of the characteristic peaks of the anatase phase decreased at a calcination temperature of 450°C, suggesting that inserting Mg and zeolite into the structure of TiO_2 slightly decreased the crystallinity of the sample [10-11]. At a higher calcination temperature, i.e., 600 °C, the characteristic peaks of the rutile phase (2θ = 26.4˚, 37˚, and 56˚) were observed to be more intense. Jansson *et al.* also reported an increase in the rutile phase as the calcination temperatures increased above 500 °C [25]. J. Krysa *et al.* [7] reported that at a calcination temperature of 900 °C, a pure rutile phase was formed in the synthesized TiO_2. The formation of a rutile phase can reduce the photocatalytic activity of this sample. Fig. 4 also shows that for the sample synthesized at a calcination temperature of 600 °C, the diffraction peak appearing at around 2θ = 33˚ can be assigned to the formation of $MgTiO_3$. This diffraction peak is in agreement with JCPDS No. 06-0494 and with those previously reported in the literature [9].

The average crystallite size of the TiO_2:Mg^{2+}/zeolite sample with the highest photocatalytic performance (T = 450 °C and 4.711 wt% of Mg) was calculated as 53.33 nm using the Scherrer equation $D = 0.9\lambda/(\beta cos\theta)$, where D is the crystal size of the sample, λ is the X-ray wavelength (0.154 nm), β is the full width at half maximum, and θ is the diffraction angle. The results of the XRF analysis of this sample are shown in Table 1. Based on Table 1, the contents of Mg, Si, and Al in the TiO_2:Mg^{2+}/zeolite sample are 4.711, 7.273, and 1.296%, respectively.

3.2. FT-IR spectrum analysis

Fig. 5 illustrates the FT-IR spectra of the TiO_2:Mg^{2+}/zeolite photocatalyst synthesized with different amounts of magnesium nitrate. As shown in Fig. 5, an absorption band is observed at around 991 cm^{-1}. This absorption band may have originated from the Ti–O stretching vibration [26]. Furthermore, the spectrum around 991 cm^{-1} can be attributed to the internal asymmetric stretching vibration of Si–O–Si or Si–O–Al in the zeolite structure [27]. The intensity of this peak changed when the amount of Mg was increased, which is attributed to the substitution of Mg with titanium or silicon. The peaks around 1250 cm^{-1} can be attributed to the unsymmetrical internal stretching vibration of C–O [28]. The peak around 1400 cm^{-1} indicates the stretching vibrations of Ti–O–Ti [18]. For this case, it seems that

Table 1. The results of the XRF analysis of the TiO_2:Mg^{2+}/zeolite sample synthesized at T = 450 °C and 4.711% of Mg.

Elements	Weight percentage (%)
S	0.155
Mg	4.711
Cl	0.058
Fe	0.198
K	0.240
Ca	0.897
Al	1.296
Si	7.273
Ti	85.112
moisture	0.060

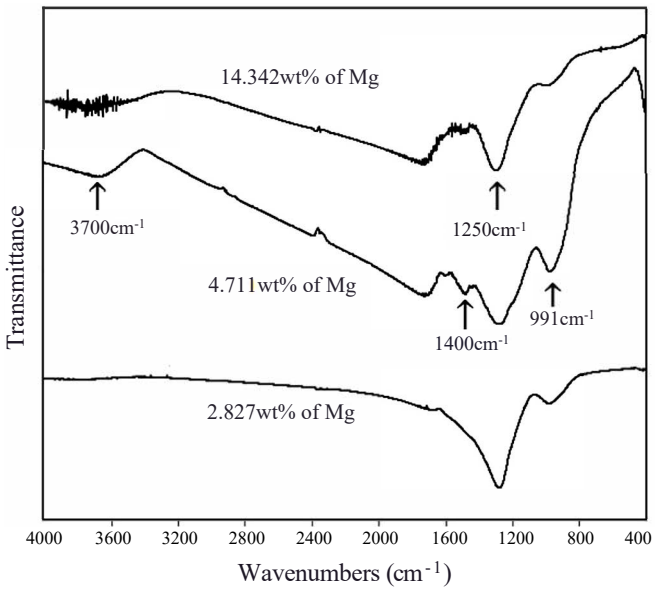

Fig. 5. The FT-IR spectra of the catalyst TiO_2:Mg^{2+}/zeolite synthesized with different amounts of Mg.

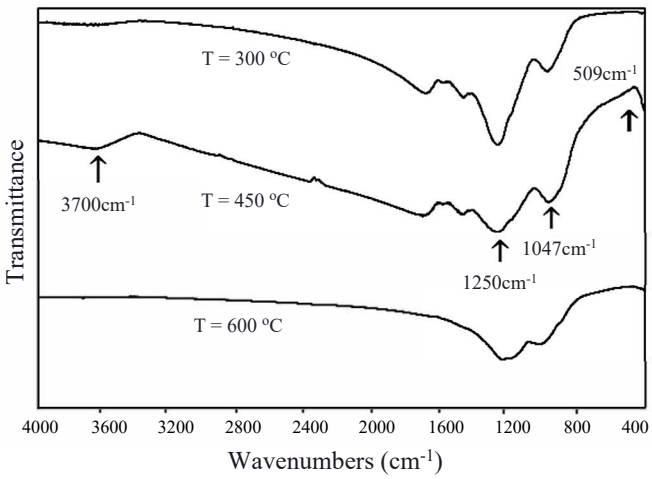

Fig. 6. The FT-IR spectra of the catalyst TiO_2:Mg^{2+}/zeolite synthesized at various calcination temperatures.

the Mg was substituted by titanium in the sample with 4.711 wt% of Mg. The peak at approximately 3700 cm^{-1} is attributed to the hydroxyl group that is present in the adsorbed water of these materials [29].

Fig. 6 shows the FT-IR spectra of the TiO_2:Mg^{2+}/ zeolite composite synthesized at various calcination temperatures. The observed peak in the 509 cm^{-1} region is related to the Ti–O–Ti vibration [23]. The absorption peak at 1047 cm^{-1} corresponds to Si(Al)–O vibrations in natural zeolite. The expansive peak in the range of 3150-3700 cm^{-1} is assigned to the hydroxyl group, which is present in the water of the zeolite structure and disappears at high temperatures [19].

3.3. FE-SEM analysis

Figs. 7-9 demonstrate the FE-SEM images of the samples. According to Fig. 7(a), the morphology of clinoptilolite zeolite is composed of a large-particle-size distribution with irregular shapes and a folded and rough surface. As shown in Fig. 7(b), spherical TiO_2 with a uniform shape was synthesized, suggesting that the surface of the synthesized TiO_2 was relatively smooth.

Fig. 8 presents the FE-SEM image of the samples synthesized at different amounts of Mg. As seen in Fig. 8, no clear variation of particle shapes was observed, but the size and size distribution of particles were a little changed. Also, no considerable change in the porosity can be observed.

Fig. 9 illustrates the FE-SEM image of the samples synthesized at various calcination temperatures. As seen from Fig. 9, the calcination temperature has a visual effect on the particle size. It As can be seen, a higher temperature would be suitable for larger particle sizes of the composite.

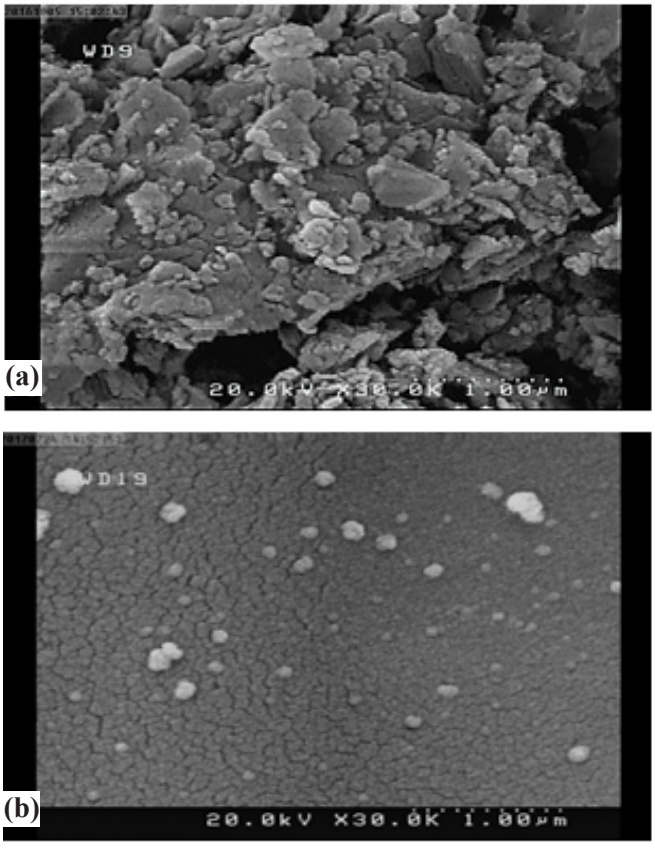

Fig. 7. EFE-SEM micrographs of (A) clinoptiolite zeolite and (B) titanium dioxide.

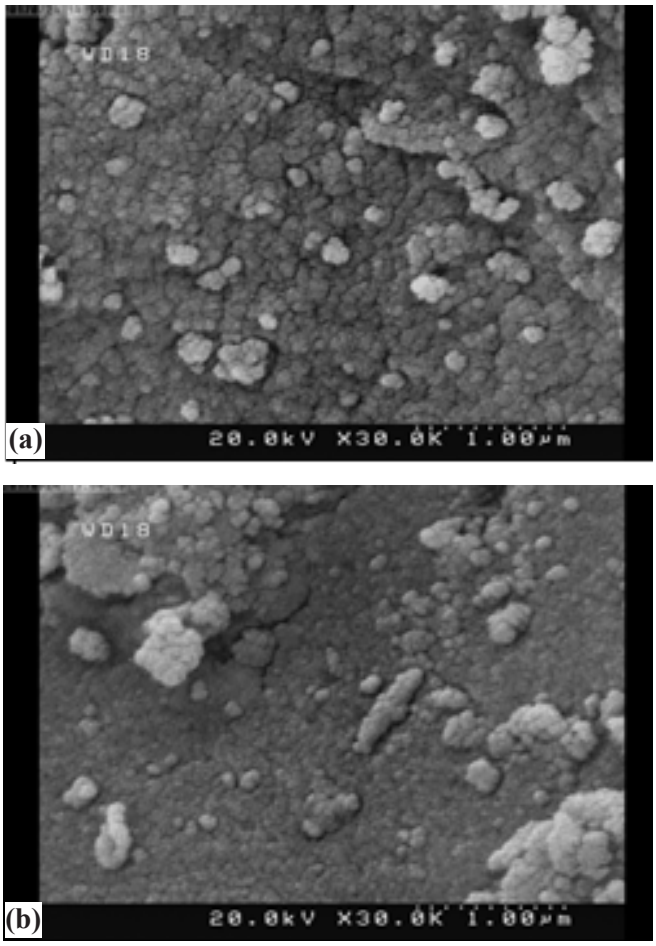

Fig. 8. FE-SEM images of TiO_2:Mg^{2+}/zeolite composites synthesized with (a) 2.827 wt% of Mg and (b) 14.342 wt% of Mg.

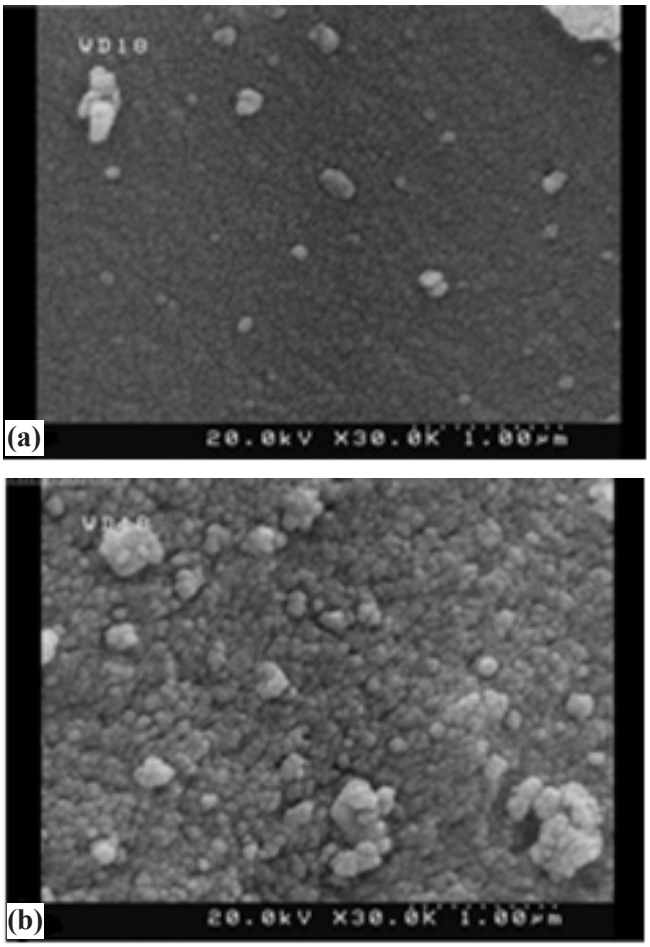

Fig. 9. FE-SEM images of TiO_2:Mg^{2+}/zeolite (4.711 wt% of Mg) composites synthesized at various calcination temperatures: (a) 450°C and (b) 600 °C.

3.4. Photocatalytic degradation of methyl orange

3.4.1. Effect of the amount of Mg

For comparison, the results of the photocatalytic activities of the degradation of methyl orange over TiO_2, TiO_2/zeolite, and TiO_2:Mg^{2+}/zeolite as-prepared samples in the same conditions under visible light are summarized in Table 2. Obviously, as shown in Table 2, the photocatalytic activity of pure TiO_2 for the degradation of methyl orange was low (57.82%). This weak performance refers to the recombination of the generated electron (e^-)-hole (h^+) pairs by visible light on the surfaces of TiO_2. The photocatalytic activity for the degradation of methyl orange was enhanced by TiO_2-containing zeolite or the addition of magnesium to the TiO_2-containing zeolite with the removal percentage of 83.29% and 97.37%, respectively. It seems that the addition of zeolite (mostly consisting of SiO_2 and Al_2O_3) and Mg with TiO_2 reduced the recombination of electron-hole, and then active species such as hydroxide radicals (OH^-), superoxide radicals (O^{2-}), and hydrogen peroxide (H_2O_2) worked to disrupt the methyl orange structures. A similar result on the mechanism of photocatalytic experiments was reported by Arabnezhad *et al.* [30].

Moreover, the results of TiO_2:Mg^{2+}/zeolite were better than those of TiO_2/zeolite in the same conditions, suggesting that the combination of Mg with TiO_2/zeolite was helpful in the improvement of the photocatalytic capability of the TiO_2/zeolite composite. Fig. 10 illustrates the effect of Mg content in the TiO_2:Mg^{2+}/

Table 2. The performance of different photocatalyst for degradation of methyl orange in the same conditions.

Photocatalyst	Removal percentage (%)
TiO_2	57.82
TiO_2/zeolite	83.29
TiO_2:Mg^{2+}/zeolite	97.37

Conditions: dosage: 5 g/l; methyl orange concentration: 10 mg/l; pH: 6; irradiation time: 50 min.

zeolite composites on the photocatalytic degradation of methyl orange. It is clear that the removal percentage of methyl orange increases with the increase in the amount of Mg, reaching a maximum at 4.711 wt% of Mg (97.37%), and then decreasing with the further increases of the amount of Mg. It seems that the electrons produced on the titanium dioxide surface by visible light move to the Mg^{2+} particle surface, thereby reducing the recombination of photogenerated electron (e^-)-hole (h^+) pairs, and then significantly increasing the photocatalytic performance.

Comparing the results of Fig. 10 and Table 1, we see that adding a certain amount of Mg reduced some impurities of natural zeolite, such as chlorine; therefore, increased the performance of the photocatalyst.

It can also be observed that by adding more than the appropriate amount of Mg, the conglomeration of Mg^{2+} particles caused the recombination of electron and hole pairs, resulting in a declined photocatalytic activity. For the sake of comparison, the sample of TiO_2:Mg^{2+}/zeolite with 4.711 wt% of Mg was used in the following experiments.

3.4.2. Effect of calcination temperatures

In order to investigate the effect of calcination temperature on the photocatalytic activity of the TiO_2:Mg^{2+}/zeolite composite, the photocatalytic degradation of methyl orange over synthesized composites calcinated at 300-600 °C was studied under visible light and the results were displayed in Fig. 11. As shown in Fig. 11, the removal percentage of methyl orange increases with the increase of the calcination temperature. Furthermore, the maximum removal percentage for TiO_2:Mg^{2+}/zeolite composite (97.73%) was obtained at 450 °C, and decreased as the calcination temperature increased to 600°C.

As mentioned in XRD analysis, when the calcination temperature is over 450°C, the anatase phase, which is useful due to its higher photocatalytic efficiency, is decreased and the amount of the rutile phase is increased, in line with the results reported in [31]. For comparison, the sample of TiO_2:Mg^{2+}/zeolite calcinated at 450°C was utilized in the following experiments.

3.4.3. Effect of photocatalyst loading

The catalyst concentration is a highly significant parameter in wastewater treatment. The influence of various initial composite concentrations (from 2 to 7 g/l) on the photodegradation of methyl orange has been examined at constant dye concentration (10 mg/l, pH=6) and irradiation time (50 min). The removal percentage of methyl orange over the TiO_2:Mg^{2+}/zeolite composite is illustrated in Fig. 12. The results demonstrate that, by increasing the amount of photocatalyst up to 5

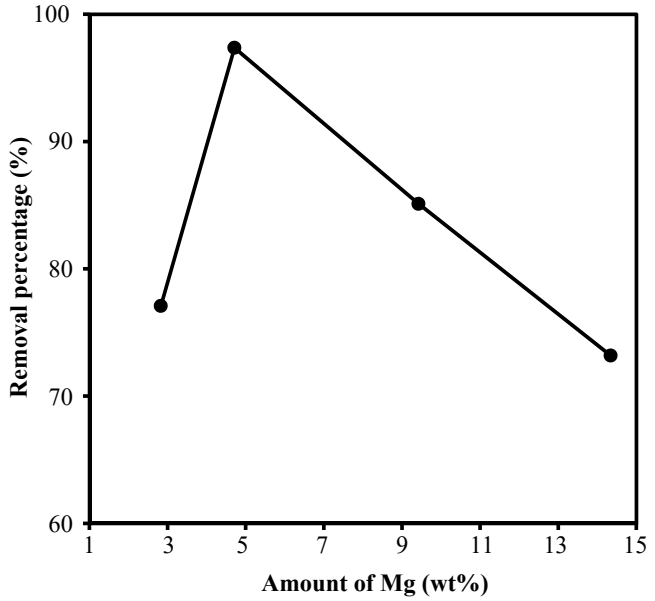

Fig. 10. The effect of the amount of Mg in TiO_2:Mg^{2+}/zeolite composites on photodegradation of methyl orange. Dosage of catalyst: 5 g/l, methyl orange concentration: 10 mg/l, pH: 6, irradiation time: 50 min.

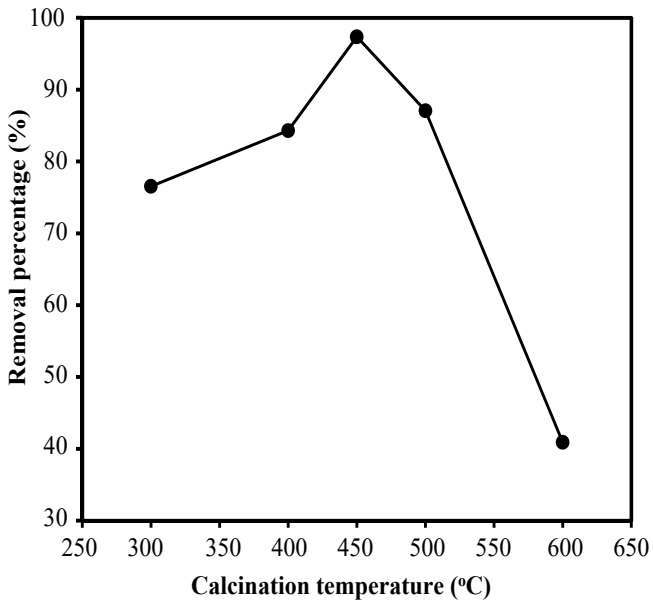

Fig. 11. The effect of calcination temperature on photodegradation of methyl orange over TiO_2:Mg^{2+}/zeolite composites. Dosage of catalyst: 5g/l, methyl orange concentration: 10 mg/l, pH: 6, irradiation time: 50 min.

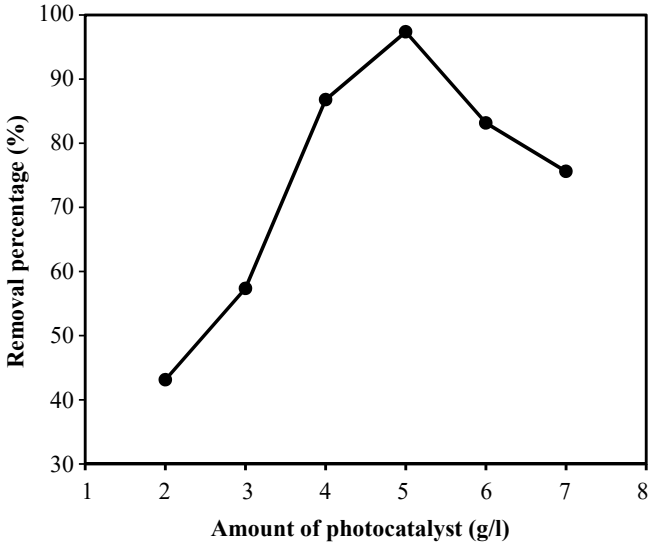

Fig. 12. The effect of the amount of photocatalyst on photodegradation of methyl orange over TiO_2:Mg^{2+}/zeolite composites. Methyl orange concentration: 10 mg/l, pH: 6, irradiation time: 50 min.

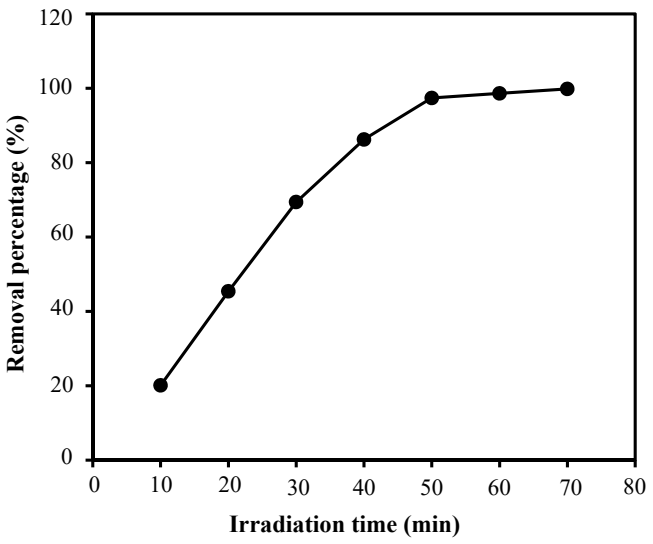

Fig. 13. The effect of irradiation time on photodegradation of methyl orange over TiO_2:Mg^{2+}/zeolite composites. Methyl orange concentration: 10 mg/l, pH: 6, dosage of catalyst: 5 g/l.

g/l, the photodegradation of methyl orange increases with a trend similar to that reported in [32]. In fact, by increasing the number of composite particles, the number of photons absorbed on the surface of the composite increased, leading to the enhancement of the methyl orange degradation.

As shown in Fig. 12, at above 5 g/l of photocatalyst loading, the photodegradation of methyl orange decreased with increasing catalyst concentration. This suggests that at higher amounts of photocatalyst concentration, the agglomeration of particles increases, and the active sites of composite for methyl orange photodegradation decreases. Also, an increase in photocatalyst loading beyond 5 g/l leads to the enhancement of the turbidity of the solution, reducing the irradiation field due to an increase in light scattering.

3.4.4. Effect of irradiation time

The effect of irradiation time on the photodegradation of methyl orange at the initial concentration of 10 mg/l, pH=10, and 5 g/l of catalyst dosage is displayed in Fig. 13. It is clearly seen that photodegradation increases from 20.09 to 99.82% with the irradiation time increasing from 10 to 70 min. It is evident that the rate of removal percentage of methyl orange decreased after 50 min of irradiation.

In fact, by increasing the irradiation time, the amount of photons absorbed on the surface of the photocatalyst was increased, thereby enhancing the degradation rate. At longer times, the slow rate of methyl orange degradation is attributed to the difficulty in converting the N-atoms of methyl orange into oxidized nitrogen materials [33].

3.4.5. The Effect of pH

The pH of the solution has a significant effect on the degradation of methyl orange. To study the effect of pH, the pH of methyl orange solution was scheduled to be 4, 6, 8, 10, and 12 at a constant dye concentration (20 mg/l) and irradiation time (50 min) with the results presented in Fig. 14. As seen in Fig. 14, the removal percentage of methyl orange equaled 63.21, 65.73, 83.79, 100, and 90.08% at the pH of 4, 6, 8, 10, and 12, respectively. It is evident that the degradation rate is higher in an alkaline condition than in an acidic condition. Similar results were reported in the literature regarding the photodegradation of dye solution [34-35]. In general, the surface properties of photocatalysts, such as surface-charged properties, are affected by pH variation. At low pH values, the agglomeration of photocatalyst particles reduces dye adsorption and light penetration, and the removal percentage subsequently decreased.

It has been reported that hydroxyl radical attacks on the dye molecule play a significant role in the photocatalytic degradation of methyl orange [35]. In an acidic medium (low pH), the interaction of azo linkage (-N=N-) in the methyl orange structure with hydroxyl radical was decreased due to the high concentration of

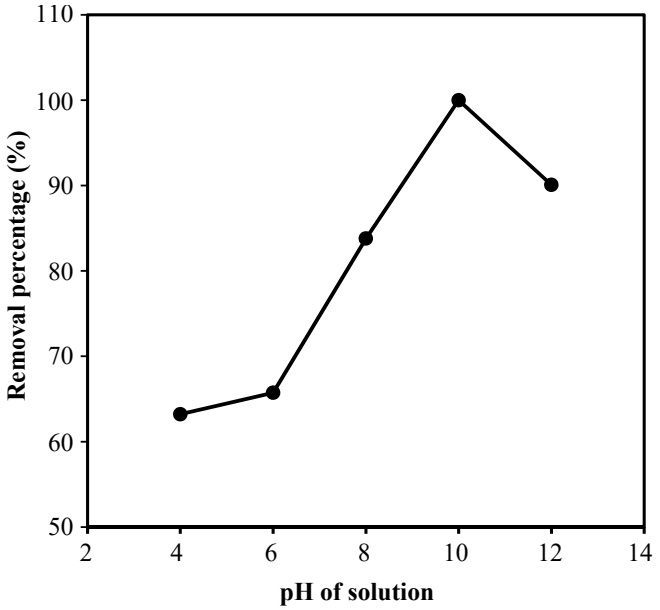

Fig. 14. The effect of pH on photodegradation of methyl orange over TiO_2:Mg^{2+}/zeolite composites. Dosage: 5 g/l, methyl orange concentration: 20 mg/l, irradiation time: 50 min.

H^+ and the interaction of excess H^+ with azo linkage, decreasing the electron densities in the azo group and reacting with the hydroxyl radical. This phenomenon decreased the removal percentage of methyl orange in the acidic medium. The photocatalytic activity of the composite was observed to be higher in alkaline condition. It seems that the presence of excess OH^- ions in an alkaline pH range caused the formation of more hydroxyl radicals (interaction between the negative surface of the composite with OH^- ions and photogenerated holes), enhancing the hydroxyl radical attack on the methyl orange molecule and improving the photocatalytic performance. Sakthivel *et al.* observed a similar behavior in their studies [36].

3.4.6. Reusability of photocatalyst

The reusability of a photocatalyst plays a significant role in its practical applications. In this study, the reusability of TiO_2:Mg^{2+}/zeolite composites was checked for five photodegradations of methyl orange cycles. For this purpose, the photodegradation of methyl orange was performed at a constant methyl orange concentration (10 mg/l with pH of 6), catalyst loading (5 g/l), and 50 min of irradiation time. In each experiment, the composites were recycled after washing, filtrating, and heating treatment at 200 °C for 2 h. The results are presented in Table 3. It is clear that the removal percentage of methyl orange slightly decreased from 96.69 to 82.06%. Therefore, there is no significant loss in the photocatalytic activity of the TiO_2:Mg^{2+}/zeolite composites in recycling experiments. It seems that repeating the photocatalytic experiments led to the loss of TiO_2 or Mg^{2+} from the surface of the composite, so the photodegradation of methyl orange was decreased. The resulting photocatalytic reusability was almost in accordance with the work of Shahmirzaee *et al.* [37]. Also, heat treatment can cause the agglomeration of composite particles, thus reducing the removal percentage of methyl orange.

4. Conclusion

In this study, a TiO_2:Mg^{2+}/zeolite composite was synthesized by the sol-gel technique and used as a photocatalyst for the degradation of methyl orange as an organic pollutant. Results showed that the addition of Mg to TiO_2/zeolite is useful due to its appropriate performance in the effective separation of electron and hole pairs and the enhancement of the photocatalyst activity of the composite. The appropriate content of Mg in the composite was obtained as 4.711 wt% with a removal percentage of methyl orange of 100 % under 50 min of irradiation time. In addition, results indicated that the sample obtained at the calcination temperature of 450 °C showed the highest amount of anatase phase for the TiO_2 structure and removal efficiency. Furthermore, the experimental results of the prepared composite photocatalytic degradation of methyl orange indicated that the degradation rate was higher in an alkaline condition than in an acidic condition due to the formation of more hydroxyl radicals. Therefore, we can conclude that the photocatalyst was stable and provides suitable reusability.

Table 3. Reusability of the TiO_2:Mg^{2+}/zeolite in photodegradation of methyl orange.

Run	Removal percentage (%)
1	96.69
2	93.21
3	89.39
4	86.17
5	82.06

Dosage: 5 g/l; methyl orange concentration: 10 mg/l; pH: 6; irradiation time: 50 min.

References

[1] K. Guesh, A. Mayoral, C. Marquez-Alvarezd, Y. Chebude, I. Diaz, Enhanced photocatalytic activity of TiO_2 supported on zeolites tested in real wastewaters from the textile industry of Ethiopia, Micropor. Mesopor. Mat. 225 (2016) 88-97.

[2] N. Setthaya, P. Chindaprasirt, Sh. Yin, K. Pimraksa, TiO_2-zeolite photocatalysts made of metakaolin and rice husk ash for removal of methylene blue dye, Powder Technol. 313 (2017) 417-426.

[3] Y. He, H. Lin, Y. Dong, Q. Liu, L. Wang, Simultaneous removal of ammonium and phosphate by alkaline-activated and lanthanum-impregnated zeolite, Chemosphere, 164 (2016) 387-395.

[4] A. Ates, G. Akgul, Modification of natural zeolite with NaOH for removal of manganese in drinking water, Powder Technol. 287 (2016) 285-291.

[5] A. Ates, C. Hardacre, The effect of various treatment conditions on natural zeolites: Ion exchange, acidic, thermal and steam treatments, Adv. Colloid Interfac. 372 (2012) 130-140.

[6] M. Bahrami, A. Nezamzadeh-Ejhieh, Effect of supporting and hybridizing of FeO and ZnO semiconductors onto an Iranian clinoptilolite nano-particles and the effect of ZnO/FeO ratio in the solar photodegradation of fish ponds waste water, Mat. Sci. Semicon. Proc. 27 (2014) 833-40.

[7] J. Krysa, M. Keppert, J. Jirkovsky, V. Stengl, J. Subrt, The effect of thermal treatment on the properties of TiO_2 photocatalyst, Mater. Chem. Phys. 86 (2004) 333-339.

[8] M.A. Aramendia, V. Borau, C. Jimenez, A. Marinas, J.M. Marinas, J.R. Ruiz, F.J. urbano, Magnesium-containing mixed oxides as basic catalysts: base characterization by carbon dioxide TPD-MS and test reactions, J. Mol. Catal. A-Chem. 218 (2004) 81-90.

[9] E.A.V. Ferri, J.C. Sczancoski, L.S. Cavalcante, E.C. Paris, J.W.M. Espinosa, A.T. de Figueiredo, P.S. Pizani, V.R. Mastelaro, J.A. Varela, E. Longo, Photoluminescence behavior in $MgTiO_3$ powders with vacancy/distorted clusters and octahedral tilting, Mater. Chem. Phys. 117 (2009) 192-198.

[10] W.L. Jin, J.X. Gao, H.S. Chen, F.X. Zeng, Z.G. Zhang, N.J. Liu, J. Guan, Photocatalytic reduction of nitrate ion in drinking water by using metal-loaded $MgTiO_3$-TiO_2 composite semiconductor catalyst, J. Photoch. Photobio. A, 162 (2004) 585-590.

[11] H. Baniamerian, S. Shokrollahzadeh, Improvement in photocatalysts and photocatalytic reactors for water and wastewater treatment: A review, J. Particle Sci. Technol. 2 (2016) 119-140.

[12] M. Rezaei, M. Khajenoori, B. Nematollahi, Preparation of nanocrystalline MgO by surfactant assisted precipitation method, Mater. Res. Bull. 46 (2011) 1632-1637.

[13] Th. Perraki, A. Orfanoudaki, Mineralogical study of zeolites from Pentalofos area, Thrace, Greece, Appl. Clay Sci. 25 (2004) 9-16.

[14] Y. Kim, M. Yoon, TiO_2/Y-Zeolite encapsulating intramolecular charge transfer molecules: a new photocatalyst for photoreduction of methyl orange in aqueous medium, J. Mol. Catal. A-Chem. 168 (2001) 257-263.

[15] P. Thuadaij, K. Pimraksa, A. Nuntiya, Synthesis of high cation exchange capacity Faujasite from high calcium fly Ash, Aust. J. Bas. Appl. Sci. 6 (2012) 194-208.

[16] A. Tadjarodi, M. Haghverdi, V. Mohammadi, Preparation and characterization of nanoporous silica aerogel from rice husk ash by drying at atmospheric pressure, Mater. Res. Bull. 47 (2012) 2584-2589.

[17] I. Kuzniarska-Biernacka, M.A. Fonseca, I.C. Neves, Manganese complexes with triazenido ligands encapsulated in NaY zeolite as heterogeneous catalysts, Inorg. Chim. Acta, 394 (2013) 591-597.

[18] D. Wu, B. Zhang, C. Li, Z. Zhang, H. Kong, Simultaneous removal of ammonium and phosphate by zeolite synthesized from fly ash as influenced by salt treatment, J. Colloid Interf. Sci. 304 (2006) 300-306.

[19] K.M. Alvarez, J. Alvarado, B.S. Soto, M.A. Hernandez, Synthesis of TiO_2 nanoparticles and TiO_2-Zeolite composites and study of optical properties and structural characterization, Optik, 169 (2018) 137-146.

[20] G. Zhang, A. Song, Y. Duan, S. Zheng, Enhanced photocatalytic activity of TiO_2/zeolite composite for abatement of pollutants, Micropor. Mesopor. Mat. 255 (2018) 61-68.

[21] R. Camposeco, S. Castillo, M. Hinojos-Reyes, I. Mejia-Centeno, R. Zanella, Effect of incorporating vanadium oxide to TiO_2, Zeolite-ZM5, SBA and P25 supports on the photocatalytic activity under visible light, J. Photoch. Photobio. A, 367 (2018) 178-187.

[22] T. Tsoncheva, L. Ivanova, C. Minchev, M. Froba,

Cobalt-modified mesoporous MgO, ZrO_2 and CeO_2 oxides as catalysts for methanol decomposition, J. Colloid. Interf. Sci. 333 (2009) 277-284.

[23] Y.X. Zhang, Y. Jia, Synthesis of MgO/TiO_2/Ag composites with good adsorption combined with photodegradation properties, Mat. Sci. Eng. B-Adv. 228 (2018) 123-131.

[24] D. Kanakaraju, J. Kockler, C.A. Motti, B.D. Glass, M. Oelgemoller, Titanium dioxide/zeolite integrated photocatalytic adsorbents for the degradation of amoxicillin, Appl. Catal. B-Environ. 166-167 (2015) 45-55.

[25] I. Jansson, S. Suárez, F. Javier Garcia-Garcia, B. Sánchez, Zeolite–TiO_2 hybrid composites for pollutant degradation in gas phase, Appl. Catal. B-Environ. 178 (2015) 100-107.

[26] Y. Kim, M. Yoon, TiO_2/Y-Zeolite encapsulating intramolecular charge transfer molecules: a new photocatalyst for photoreduction of methyl orange in aqueous medium, J. Mol. Catal. A-Chem. 168 (2001) 257-263.

[27] N. Setthaya, P. Chindaprasirt, S. Yin, K. Pimraksa, TiO_2-Zeolite photocatalysts made of metakaolin and rice husk ash for removal of methylene blue dye, Powder Technol. 313 (2017) 417-426.

[28] P. Aberoomand, S. Moradi, S. Samadi, M.S. Tehrani, M.H. Givianrad, Effect of CMC and HPC mixture on the photocatalytic activity of Nd-TiO_2/SiO_2 film under visible light irradiation, Turk. J. Chem. 35 (2011) 37-44.

[29] Q. Zhao, M. Wang, H. Yang, D. Shi, Y. Wang, Preparation, characterization and the antimicrobial properties of metal ion-doped TiO_2 nano-powders, Ceram. Int. 44 (2018) 5145-5154.

[30] M. Arabnezhad, M. Shafiee Afarani, A. Jafari, Co-precipitation synthesis of ZnO-TiO_2 nanostructure composites for arsenic photodegradation from industrial wastewater, Int. J. Environ. Sci. Tech. 16 (2019) 463-468.

[31] Q. Sun, X. Hu, S. Zheng, Z. Sun, S. Liu, H. Li, Influence of calcination temperature on the structural, adsorption and photocatalytic properties of TiO_2 nanoparticles supported on natural zeolite, Powder Technol. 274 (2015) 88-97.

[32] Q. Sun, H. Li, S. Zheng, Z. Sun, Characterizations of nano-TiO_2/diatomite composites and their photocatalytic reduction of aqueous Cr(VI), Appl. Surf. Sci. 311 (2014) 369-376.

[33] E. Khaksar, M. Shafiee Afarani, A. Samimi, In Situ solvothermal crystallization of TiO_2 nanostructure on aumina granules for photocatalytic wastewater treatment, J. Mater. Eng. Perform. 23 (2014) 92-100.

[34] M. Huang, C. Xu, Z. Wu, Y. Huang, J. Lin, J. Wu, Photocatalytic discolorization of methyl orange solution by Pt modified TiO_2 loaded on natural zeolite, Dyes Pigments, 77 (2008) 327-334.

[35] M. Muruganandham, M. Swaminathan, Photocatalytic decolourisation and degradation of Reactive Orange 4 by TiO_2-UV process, Dyes Pigments, 68 (2006) 133-142.

[36] S. Sakthivel, B. Neppolian, M.V. Shankar, B. Arabindoo, M. Palanichamy, V. Murugesan, Solar photocatalytic degradation of azo dye: comparison of photocatalytic efficiency of ZnO and TiO_2, Sol. Energ. Mat. Sol. C. 77 (2003) 65-82.

[37] M. Shahmirzaee, M. Shafiee Afarani, A. Iran Nejhad, A.M. Arabi, Microwave-assisted combustion synthesis of $ZnAl_2O_4$ and ZnO nanostructure particles for photocatalytic wastewater treatment, Particul. Sci. Technol. 37 (2019) 110-117.